Dynamic generation of plasmonic Moiré fringes using phase-engineered optical vortex beam

Guanghui Yuan,[1,†] Qian Wang,[1,†] and Xiaocong Yuan[2,*]

[1]*School of Electrical & Electronic Engineering, Nanyang Technological University, 50 Nanyang Avenue, 639798, Singapore*

[2]*Institute of Modern Optics, Key Laboratory of Optical Information Science & Technology, Ministry of Education of China, Nankai University, Tianjin, 300071, China*

**Corresponding author: xcyuan@nankai.edu.cn*

Received April 10, 2012; revised May 17, 2012; accepted May 17, 2012; posted May 17, 2012 (Doc. ID 166441); published June 26, 2012

Dynamic generation of plasmonic Moiré fringes using a phase engineered optical vortex (OV) beam is experimentally demonstrated. Owing to the unique helical phase carried by an OV beam, the initial phase of surface plasmon polaritons (SPPs) emanating from a metallic grating can be adjusted dynamically by changing the phase hologram displayed on a spatial light modulator. Plasmonic Moiré fringes are readily achieved by overlapping two SPP standing waves with certain angular misalignment, excited by the positive and negative topological charge components, respectively, of a cogwheel-like OV beam. The near-field scanning optical microscopy measurement result of SPP distributions has shown a good agreement with the numerical predictions.

OCIS codes: 240.6680, 080.4865, 120.4120.

Moiré fringe refers to an interference pattern created when two grids are overlaid at an angle, or when they have slightly different mesh sizes. In classical far-field optics, the Moiré phenomenon has been extensively studied in the past several decades, showing broad applications in displacement measurement, strain analysis, and optical alignment due to its extreme sensitivity to slight distortion [1–3]. However, in the near-field counterpart, very few works have reported on Moiré fringes so far, especially on plasmonic ones. By inserting a silver slab between two subwavelength gratings to enhance the evanescent field, the contrast improvement of surface plasmon polariton (SPP)—mediated Moiré fringes has been studied, which shows potential for defect detection in semiconductor devices and ultrahigh-resolution alignment in nanofabrication techniques [4,5]. SPPs are charge-density waves that propagate along a metal/dielectric interface, featuring a highly localized electromagnetic field and short effective wavelength. Therefore, SPPs are served as a promising optical information carrier on plasmonic chips for interfacing with high-speed photonic components and small-sized electronic circuits and are widely applied for development of various plasmonic devices [6,7].

It is interesting to further explore the near-field Moiré effect by effective manipulation of SPPs with the help of specially designed nanostructures and wavefront modulated excitation beams, such as optical vortex (OV) beams. OV beams are well known for their helical wavefront characterized by a phase function of $\exp(il\varphi)$, where φ is the azimuthal angle and l is the topological charge [8,9]. The sign of l determines handedness of the helical wavefront. Due to their unique phase properties, OV beams provide a natural and simple phase modulation method to effectively and dynamically manipulate SPPs. In our previous work, various plasmonic phenomena based on OV beams have been demonstrated. SPP standing waves were experimentally excited by using linearly polarized OV beams for high-resolution and wide-field fluorescence imaging [10]. SPP dynamic focusing based on OV beams has also been proposed recently, which is beneficial for in-plane coupling and routing of SPPs on photonic chips [11]. In this Letter, we extend this phase modulation concept and experimentally demonstrate the dynamic generation of two-dimensional (2D) plasmonic Moiré fringes resulting from the overlapping of two SPP standing waves with an angular misalignment, excited by an OV beam with different topological charges. The SPP distributions are recorded by near-field scanning optical microscopy (NSOM), which are consistent with by finite-difference time-domain (FDTD) simulation results.

Figure 1(a) shows a schematic diagram of the experimental setup. The OV beam is generated by illuminating a collimated linearly polarized Gaussian beam (He-Ne Laser, wavelength 633 nm) on a phase hologram displayed on a parallel-aligned nematic liquid crystal spatial light modulator (SLM). Subsequently, the OV beam is focused onto the nanostructures by a 10× microscope objective. NSOM (NT-MDT, NTEGRA Solaris) with an aluminum-coated fiber tip of 100 nm diameter opening is used to obtain near-field distribution of the SPPs, and the optical signal is amplified by using a photo multiplier tube (PMT). A half-wave plate is used to adjust the polarization direction of the incident OV beam. In our experiment, a conventional OV beam with single topological charge and a cogwheel-like OV beam, which is the superposition of two OV beams with opposite topological charges, are used for dynamic modulation of SPPs. These two OV beams are generated by the use of a fork phase hologram and an entangled double-helix phase pattern on an SLM, respectively [12]. The NSOM recorded intensity profiles of the OV beam of $l = 6$ (left) and $l = \pm 6$ (right) before incidence on the nanostructure are shown in the inset of Fig. 1, where the doughnut shape and cogwheel-like shape can readily be seen.

Figure 2(a) displays the scanning electron microscopy (SEM) graph of a 30 μm long grating consisting of five subwavelength slits with a period of 610 nm and a slit width of 240 nm embedded in a 100 nm thick silver film ($\varepsilon_m = -15.89 + 1.08i$). It was fabricated by using a standard electron beam lithography (EBL; Raith e_LiNE)

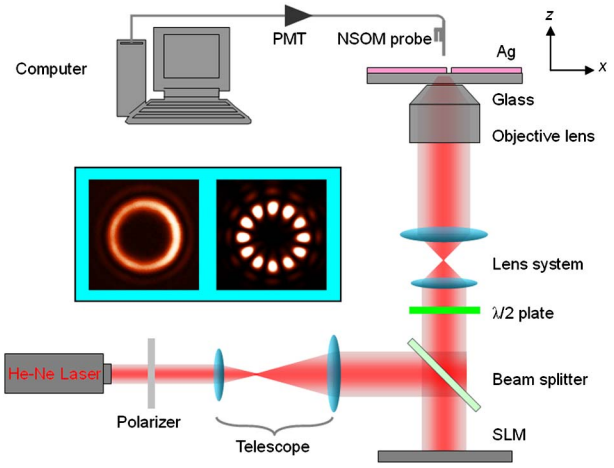

Fig. 1. (Color online) Schematic configuration of the experimental setup, where a phase hologram is coded on an spatial light modulator (SLM) to generate OV beams with various topological charges and NSOM is used to capture the SPP distributions. The inset shows the NSOM-measured intensity profiles of two types of incident OV beams: (left) a common OV beam of $l = 6$ and (right) a cogwheel-like OV beam of $l = \pm 6$.

technique followed by thermal evaporation and a lift-off process. An x-polarized OV beam of $l = 6$ is utilized as the incident beam. The inset of Fig. 2(b) shows its phase distribution as six segments, linearly increasing from 0 (blue) to 2π (red) along the azimuthal direction in each segment. Obviously, when the intensity maxima of such an OV beam shine on the sub wavelength grating, there is a positive phase accumulation from the bottom up along the grating direction. Since the subwavelength slits sustain only a fundamental mode, the beam experiences the same phase delay after passing through the grating. The helical phase of the incident OV beam is transferred to the SPPs emanating from different parts of the grating. Therefore, the excited SPP will propagate along the direction indicated by the blue arrows with a positive tilt angle of around 9.5 deg, as shown in Fig. 2(b). The fringes around the grating are caused by interference between a directly transmitted beam and leftward or rightward propagating SPPs. At the left side, in addition to the apparent SPP fringes, some interesting phenomena are seen: there are no fringes at the beam center because of the definite zero intensity of the OV beam; a fork fringe dislocation is found between the top and bottom SPP fringes with a number difference of 6, which is intrinsically determined by the value of topological charge l. Moreover, the larger the topological charge, the bigger the tilt angle. In this way, the excited plasmonic field can dynamically be manipulated accordingly by changing the phase information encoded on SLM in real time.

To further study the dynamic control capability and generate plasmonic Moiré fringes, another nanostructure consisting of four subwavelength gratings is fabricated by EBL, and its SEM graph is depicted in Fig. 3(a). Here the thickness of silver film is increased to 150 nm to effectively block the direct transmission beam, and the incident OV beam is polarized along the diagonal direction (black arrow) in order to excite SPPs at the four gratings simultaneously. Based on the identical phase modulation scheme illustrated in Fig. 2, the propagation direction of SPPs emanating from the gratings in the central region tilt clockwise (red solid arrows) and counterclockwise (blue dashed arrows) under the excitation of positive and negative topologically charged OV beams, respectively. These four SPPs interfere with each other either constructively or destructively, resulting in the formation of a 2D plasmonic spot array with a period of 425 nm and FWHM of 212 nm for each spot. Figures 3(b) and 3(c) show the SPP distributions under OV illuminations of $l = 6$ and $l = -6$, respectively. In comparison with 2D SPP standing waves generated by linearly polarized Gaussian beam illumination [13,14], the use of OV beams represents distinctive features: the standing waves have an angular rotation, clockwise for positive

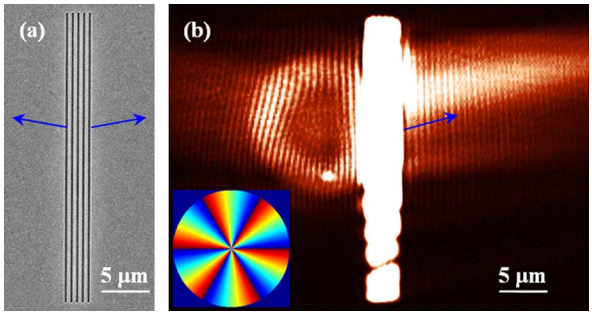

Fig. 2. (Color online) (a) Scanning electron microscopy image of the metallic grating: length 30 μm, period 610 nm, and slit width 240 nm. The thickness of silver film is 100 nm; (b) NSOM-measured SPP distributions under the illumination of an OV beam of $l = 6$. The inset shows the OV beam's phase profile after normalization to 2π. The blue arrows indicate the propagating direction of SPPs with an angular displacement.

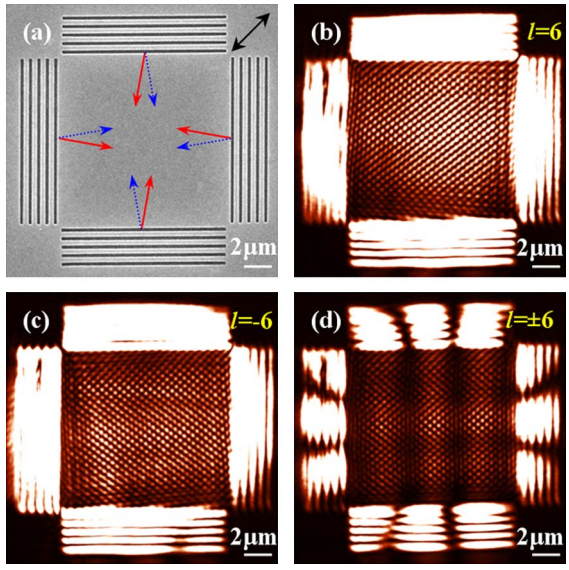

Fig. 3. (Color online) (a) SEM image of four metallic gratings to generate plasmonic Moiré fringes. The central area is 12 μm × 12 μm. Black arrow shows the polarization direction of incident OV beam. Red solid arrows and blue dashed arrows show the propagation direction of SPP excited by positive and negative topological charge OV beams, respectively. NSOM-measured 2D SPP standing waves excited by an OV beam of (b) $l = 6$ and (c) $l = -6$; (d) NSOM-recorded plasmonic Moiré fringes excited by a cogwheel-like OV beam of $l = \pm 6$.

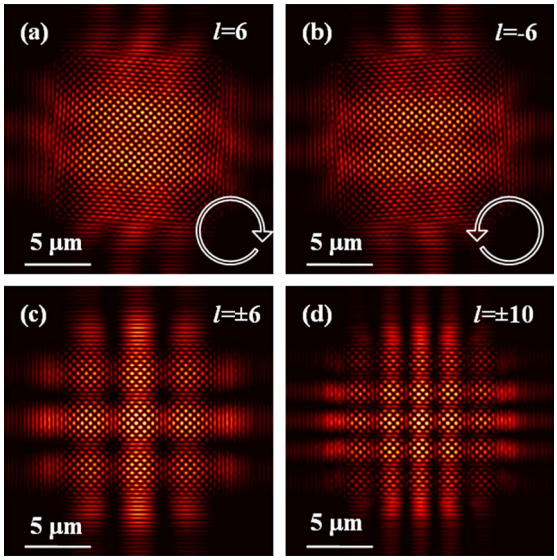

Fig. 4. (Color online) FDTD calculated 2D SPP standing waves excited by OV beams of (a) $l = 6$ and (b) $l = -6$, where the white arrows show their clockwise and counterclockwise, respectively, angular displacement directions. Plasmonic Moiré fringes excited by cogwheel-like OV beams of (c) $l = \pm 6$ and (d) $l = \pm 10$.

l and counterclockwise for negative l, which are clearly distinguished from the fringes' orientations near the gratings. Therefore, if these two 2D SPP standing waves possessing the same grid sizes and a natural angular displacement overlap with each other, it is possible to generate 2D plasmonic Moiré fringes. To this end, two OV beams should be used in the experiment and be aligned coaxially. However, it is difficult to align two OV beams along the same optical path and precisely control their relative phase. Fortunately, this puzzle is circumvented by properly coding two topologically charged components onto a phase hologram to produce a single structured OV beam, such as the cogwheel-like OV beam with opposite topological charges discussed above. The NSOM-measured experimental result of plasmonic Moiré fringes using a cogwheel-like OV beam of $l = \pm 6$ is given in Fig. 3(d), where the period of Moiré fringes is measured to be 3.85 μm.

FDTD simulations are carried out to verify our experimental findings. Using the same structure in Fig. 3(a), the near-field SPP intensity distributions under the illumination of OV beams of $l = 6$, -6, and ± 6 are shown in Fig. 4(a)–4(c), respectively, which agree well with their corresponding counterparts in Fig. 3(b)–3(d). Due to their mixing, plasmonic Moiré fringes consisting of a 3×3 array with an augmented period of 4 μm are found in Fig. 4(c). For larger topological charges, plasmonic Moiré fringes with more complex distributions can be formed. For example, if a topological charge of ± 10 is utilized, a 5×5 spot array with a smaller period of 2.4 μm is formed due to the larger angle shift between the 2D SPP standing waves generated by OV beams of $l = 10$ and -10. Further investigation shows that the period of Moiré fringes is inversely proportional to the angular displacement between the two sets of SPP standing waves.

In conclusion, we experimentally demonstrated a method for dynamic generation of plasmonic Moiré fringes using phase-modulated OV beams illuminating on metallic nanostructures. By proper design of the constituent topological charges encoded in the phase hologram, the plasmonic Moiré fringes with distinctive features can be dynamically varied. The experimental results of SPP distributions recorded by NSOM measurement agree well with the numerical predictions. The proposed method provides a unique and flexible way to generate plasmonic fringes in a dynamic and reconfigurable fashion and has potential for defect detection on plasmonic chips, surface plasmon holography [15], and nanofabrication field.

This work was partially supported by the National Natural Science Foundation of China under grant nos. 10974101, 61036013, and 61138003; the Ministry of Science and Technology of China under grant no. 2009DFA52300 for China—Singapore collaborations; and the National Research Foundation of Singapore under grant no. NRF-G-CRP 2007-01. X.C.Y. acknowledges the support given by Tianjin Municipal Science and Technology Commission under grant no. 11JCZDJC15200.

†Authors with equal contribution

References

1. K. Creath, J. Schmit, and J. C. Wyant, *Optical Shop Testing*, D. Malacara, ed. (Wiley, 2007), p. 756.
2. K. Patorski and M. Kujawinska, *Handbook of the Moiré Fringe Technique* (Elsevier, 1993).
3. C. A. Walker, *Handbook of Moiré Measurement* (IoP, 2004).
4. Z. W. Liu, S. Durant, H. Lee, Y. Xiong, Y. Pikus, C. Sun, and X. Zhang, Opt. Lett. **32**, 629 (2007).
5. F. B. Deng, C. L. Du, and X. G. Luo, J. Opt. Soc. Am. B **25**, 443 (2008).
6. E. Ozbay, Science **311**, 189 (2006).
7. W. L. Barnes, A. Dereux, and T. W. Ebbesen, Nature **424**, 824 (2003).
8. D. L. Andrews, *Structured Light and its Applications* (Elsevier, 2008).
9. J. F. Nye and M. V. Berry, Proc. R. Soc. A **336**, 165 (1974).
10. P. S. Tan, X.-C. Yuan, G. H. Yuan, and Q. Wang, Appl. Phys. Lett. **97**, 241109 (2010).
11. G. H. Yuan, X.-C. Yuan, J. Bu, P. S. Tan, and Q. Wang, Opt. Express **19**, 224 (2011).
12. D. W. Zhang and X.-C. Yuan, Opt. Lett. **28**, 1864 (2003).
13. Z. W. Liu, Q. H. Wei, and X. Zhang, Nano Lett. **5**, 957 (2005).
14. Q. Wang, J. Bu, and X.-C. Yuan, Opt. Express **18**, 2662 (2010).
15. M. Ozaki, J. Kato, and S. Kawata, Science **332**, 218 (2011).